Appl Nanosci (2012) 2:311–317
DOI 10.1007/s13204-012-0119-3

ORIGINAL ARTICLE

Investigations on nanocrystalline BST-LSMO magnetodielectric composites

M. M. Sutar · A. N. Tarale · S. R. Jigajeni · S. B. Kulkarni · P. B. Joshi

Received: 17 November 2011 / Accepted: 7 April 2012 / Published online: 6 May 2012

Abstract The paper reports the synthesis of $Ba_{1-x}Sr_xTiO_3$ (BST) for $x = 0.20$, 0.25, and 0.30 via hydroxide co-precipitation route to result into the BST nanoparticles of size nearly 50 nm. The $La_{0.67}Sr_{0.33}MnO_3$ (LSMO) is also synthesized using co-precipitation route to achieve nanocrystaline particles. Further, the magnetodielectric (MD) composites of BST0.20, BST0.25, and BST0.30 are formed by addition of the LSMO at $y = 0.1$ and 0.2. The parent BST compositions are analysed for its dielectric properties. The composite LSMO-BST (LBST) is investigated for the variation of dielectric constant and impedance spectra as a function of applied magnetic field for the frequency between 500 Hz to 1 MHz. The observations on MD effect show that the dielectric constant possesses contributions due to magnetic field dependant interfacial polarization and variations due to the induced stress.

Keywords BST · LSMO · Ferroelectric · Magnetodielectric composites · Magneto-capacitance

Introduction

$Ba_{1-x}Sr_xTiO_3$ (BST) is a well-known ferroelectric material where the transition temperature (T_c) could be reduced nearly from 120 °C down to −231 °C by varying x between 0 and 1 (McCormick et al. 2001). The compounds with x in the vicinity of 0.30 are of special interest owing to its $T_c = 30$ °C (≈RT) and very high value of dielectric constant (ε) in the vicinity of T_c in both ferroelectric and paraelectric regions (McCormick et al. 2001; Ianculescu et al. 2008; Zimmerman et al. 2004; Chien et al. 1999). BST with $x = 0.30$, i.e. $Ba_{0.70}Sr_{0.30}TiO_3$, is known to possess useful value of electrical tunability $\{\varepsilon(E) - \varepsilon(0)\}/\varepsilon(0)$. Therefore, BST finds its applications in tunable filters, tunable dielectric resonators, multilayer capacitance devices, etc. (Haeni et al. 2004; Tagantsev et al. 2003; Fuck and Dorman 2006; Jain et al. 2003). As far as the magnetoelectric (ME) and magnetodielectric (MD) properties are concerned it is expected that ME and MD coefficients will be high in the ferroelectric region and in the vicinity of Tc. It is seen that magnitudes of $d\varepsilon/dT$, i.e. rate of change of permittivity with temperature and dP_r/dT, i.e. rate of change of polarization with temperature are maximum in this region of temperature and reduce as the temperature is decreased below T_c. Further, the dP_r/dT is negative, while $d\varepsilon/dT$ is positive in the vicinity of T_c. As the ME and MD phenomena are proportional to the change of polarization as a function of applied stress, the ME/MD properties are expected to be sensitive to the compositional variations of BST for x between 0.20 and 0.30. Here the T_c for $x = 0.30$ is at 30 °C and increases to nearly 58 °C for $x = 0.20$. Therefore, $d\varepsilon/dT$ and $|dP_r/dT|$ for BST at $x = 0.25$ and 0.30 will be large as compared to their values for $x = 0.20$. Owing to the discussion above, we have selected $x = 0.20$, 0.25 and 0.30 compositions for ferroelectric phase to form the MD composites.

There are few reports on MD effect observed in the $BaTiO_3$–$LaMnO_3$, $Ba_{0.6}Sr_{0.4}TiO_3$–$La_{0.70}Ca_{0.30}MnO_3$ and other similar composites. It is observed that the magnetocapacitance (MC) equal to $\{\varepsilon(H)\text{-}\varepsilon(0)\}/\varepsilon(0)$ is maximum in

M. M. Sutar · A. N. Tarale · S. R. Jigajeni · P. B. Joshi (✉)
School of Physical Sciences, Solapur University,
Solapur 413 255, India
e-mail: drpbjoshi@rediffmail.com

S. B. Kulkarni
Institute of Science, Mumbai (MS), India

the vicinity of T_c of both the magnetic and ferroelectric constituents of the composites. The observed MC is positive and large and it is understood in terms of a model as predicted by Catalan (2006). In this case, the interfacial polarization between the ferroelectric and CMR phases changes with varying dc magnetic field (H) and therefore the dielectric constant (ε) varies with the magnetic field (H). A recent report on PZT-MZF system has shown a negative MC for low value of H and it is suggested that the negative MC may corresponds to the stress-induced variations of ε as observed by Gridnev et al. (2009).

To differentiate between these two phenomena, the BST for $x = 0.20$, 0.25 and 0.30 appears to be correct choice as discussed in the paragraph above. The $La_{0.67}Sr_{0.33}MnO_3$ (LSMO) is known to possess a phase transition and CMR effect at RT. In addition, LSMO is known to possess a giant magnetostriction (GMS) at $T = T_c$, therefore, the LSMO may exhibits both the effects viz. the CMR-induced and stress-induced effect (Shui et al. 2011).

Experimental

Synthesis of $Ba_{1-x}Sr_xTiO_3$ (BST)

The $Ba_{1-x}Sr_xTiO_3$ powders are synthesized by employing hydroxide co-precipitation route followed by ceramic process of synthesis for $x = 0.20$, 0.25 and 0.30. High purity (>99.9 %) barium acetate [$Ba(CooCH_3)_2$], strontium nitrate [$Sr(NO_3)_2$], and potassium titanium oxalate [$K_2TiO(C_2O_4)_2{\cdot}2H_2O$] are used as precursors. For complete precipitation of $Ba(OH)_2$ and $TiO(OH)_2$, the molar ratio of KOH to (BaTi) of 1.6 has been used, based on the earlier report (Lee et al. 2003). It has been observed that the $Ba(OH)_2$ and $Sr(OH)_2$ are fractionally soluble in water but insoluble in alkaline medium. Therefore, the precipitates are washed in dilute NH_4OH solution with pH $\sim$10 (Kulkarni et al. 2009). The powders are calcined at 1,000 °C for 10 h and final sintering is carried out at 1,200 °C for 12 h. For characterization of bulk BST, the pellets are also sintered in the same sintering schedule. For further discussion, the samples are denoted as BSTx for $x = 0.20$, 0.25 and 0.30.

Synthesis of $La_{0.67}Sr_{0.33}MnO_3$ (LSMO)

The $La_{0.67}Sr_{0.33}MnO_3$ (LSMO) has been synthesized by employing hydroxide co-precipitation route followed by ceramic process of synthesis. The AR-grade $La(C_2H_3O_2)_3$ H_2O, $SrNo_3$, $KMnO_4$, and $MnCl_2$ $4H_2O$ are used as precursors, while a mixture of NH_4OH and KOH is used as precipitating agent. The details of the co-precipitation route are similar as reported earlier (Kim et al. 2008; Veer et al. 2008). The precipitate formed is washed thoroughly and calcinated at 1,000 °C for 12 h to achieve complete ferrite phase formation. The LSMO powder is pelletized in the form of disc of 1.2 cm diameter using pressure of nearly 2 ton per cm^2. Further, the pellets are sintered at 1,100 °C for 10 h to achieve a dense ferrite composition.

Formation of composites

The LSMO and BST composites are formed bearing the formula:

$$y\ (\mathrm{LSMO} - \mathrm{BST}x) = y\mathrm{LSMO} + (1 - y\mathrm{BST})x$$

where $x = 0.1$, and 0.2. The sintered powder of LSMO and BST was grounded together thoroughly using ethanol as a medium in Agot Mortor and pestol. The pellets of diameter 1.2 cm are formed as discussed above. The pellets are sintered at 1,125 °C for 8 h to form desired MD composites.

The parent compositions LSMO and BST as well as their composites are investigated for the structural properties using X-ray powder diffractometer (Rigaku Miniflex). For dielectric measurements, LCR-Q meter (HP4284A) is used in the frequency range from 100 Hz to 1 MHz for temperature (T) between RT and 250 °C for measurement of C_p, tanδ as a function of frequency (F), temperature (T) for dielectric characterization of BST and magnetic field (H) up to 6,000 Oe applied for MD characterization of the composites. A radiant technology precision ferroelectric workstation used to measure the RT FE polarization hysteresis.

Results and discussion

Structural analysis

Figure 1a shows XRD spectra of the LSMO powder. It is observed that the XRD spectra are in accordance with JCPDS data (JCPDS card no.89-8098). Thus from the XRD spectra, it is revealed that the ferrite compositions were synthesized in the desired rhombohedral structure with hexagonal axes of symmetry without any detectable impurity phase. Using the XRD spectra, the lattice parameters a and c are observed to be 5.40 and 13.5 Å, respectively. Using the Scherrer's formula, the particle size is calculated and is of the order 67 nm. Here, the particle size of sintered co-precipitate is above 50 nm. This is expected because of sintering at 1,000 °C for a long time of 10 h.

Figure 1b shows the XRD spectra of BST0.25. It is observed that the degree of tetragonality (c/a) reduces from 1.008 to 1.002 as the x is varied from 0.20 to 0.30 as shown in Table 1. These results are in conform with the earlier

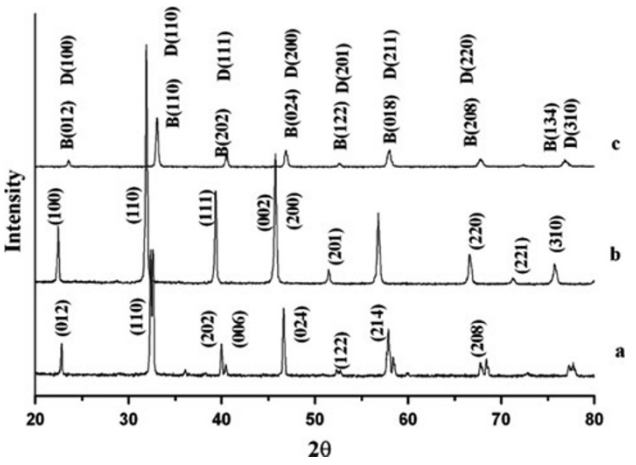

Fig. 1 XRD spectra of *a* $La_{0.67}S_{r0.33}MnO_3$; *b* $Ba_{0.75}Sr_{0.25}TiO_3$; and *c* composite (0.2) $La_{0.67}Sr_{0.33}MnO_3$–(0.8) $Ba_{0.70}Sr_{0.30}TiO_3$

Table 1 Particle size, transition temperature, lattice parameters a, c and c/a ratio for various BST compositions

Composition	*D* (nm)	T_c (°C)	*a* (Å)	*c* (Å)	*c*/*a*
$Ba_{0.80}Sr_{0.20}$ TiO_3 (BST0.20)	49	58	3.920	3.9525	1.0083
$Ba_{0.75}Sr_{0.25}$ TiO_3 (BST0.25)	65	42	3.824	3.8415	1.0046
$Ba_{0.70}Sr_{0.30}TiO_3$ (BST0.30)	62	30	3.809	3.8173	1.0022

D particle size, T_c ferroelectric transition temperature, *a and c* lattice parameters

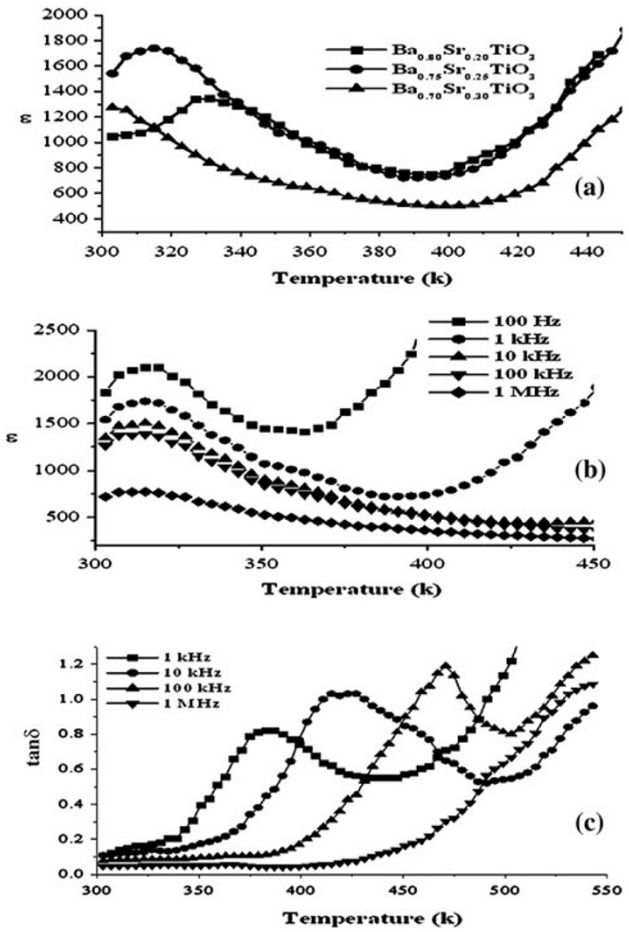

Fig. 2 **a** Variation of ε with *T* at $f = 1$ kHz for BST0.20, BST0.25 and BST0.30; **b** variation of ε versus *T* for $f = 100$ Hz, 1 kHz, 10 kHz, 100 kHz, 1 MHz (BST0.25); and **c** variation of tanδ with *T* for $f = 100$ Hz, 1 kHz, 10 kHz and 100 kHz for BST0.25

report (Ianculescu et al. 2008). The magnitudes of *a* and *c* are also in confirmation with the value reported earlier. Using Scherrer's formula, the particle size was determined to be between 49 and 65 nm (Table 1).

Figure 1c shows the XRD spectra of LBST0.30 for $y = 0.2$ composite. The peaks corresponding to the reflections of BST and LSMO could be indexed separately in Fig. 1. Thus from the XRD spectra, it could be seen that the composites formed are phase pure and possess two separate phases viz. LSMO and BST.

Dielectric properties

Figure 2a shows the variation of dielectric constant (ε) as a function of temperature (*T*) for frequency (*F*) = 1 kHz for BST0.20, BST0.25 and BST0.30. From Fig. 2a, it is seen that ε passes through a maximum at T_c. The observed T_c for BST0.20, BST0.25 and BST0.30 is shown in Table 1. Further, it is observed that ε increases with *T* again in the paraelectric region above T_c. This feature is predicted to occur because of grain–grain boundary effect (Ianculescu et al. 2008). To understand these features in detail, the ε is determined as a function of *F* and Fig. 2b shows variation of ε as a function of *T* for *F* varying between 100 Hz and 1 MHz for BST0.25, while Fig. 2c shows the variation of tanδ as a function of *T* for *F* = 100 Hz, 1, 10 and 100 kHz, respectively. Here it is observed that the increases in ε with *T* occur for frequencies below 100 kHz only and dε/dT decreases with increase in F. These features occur due to the presence of interfacial polarization at grain–grain boundary interface. The grain–grain boundary interface occurs probably due to fractional Ti^{3+} acceptor state in the bulk of grain (Bidaut et al. 1994; Choi et al. 2004). Similar features are also reported by Ianculescu et al. (2008). The observed behavior is a competitive phenomenon between the dielectric relaxation and the electrical conduction of the relaxing species.

Magnetodielectric properties

Figure 3a, b, c shows the variation of ε as a function of log*F* for LBST0.20, $y = 0.2$ and LBST0.25, $y = 0.1$ and

0.2, respectively, in the absence as well as in the presence of applied magnetic field (H). The ε is observed to decrease as a function of log$F$, where the dispersion is faster at lower frequencies as compared to the higher one. The faster decrease of ε at lower frequencies is attributed to the presence of interfacial polarization. Interfacial polarization is known to occur for BST compositions because of grain–grain boundary interaction as described earlier in the paper (Jigajeni et al. 2010). Further, the additional component of the interfacial polarization is expected to occur in the present case because of the difference of the resistivities of the LSMO and the BST phases. The LSMO is known to posses a CMR at RT and, therefore, the resistivity of LSMO phase is expected to decrease with increase in the value of applied magnetic field (H) (Urushibara et al. 1995; Yan-KunTang et al. 2006). As the resistivity decreases with H, the interfacial polarization should increase with applied magnetic field. This phenomenon is known to cause the Catalon type contribution to MC as reported earlier (Catalan 2006).

As reported recently, the another competitive phenomenon which causes the magneto-capacitance(MC) is the magnetostriction-induced variation in the ε. Due to the stress induced by the magnetostriction, it is known that the polarization of the ferroelectric phase increases, while the ε decreases with the applied stress, i.e. with increase in H. This phenomenon was reported earlier in the case of PZT-MZF bilayer ME composites. The Gridnev explained this phenomenon on the basis of Landau thermodynamic theory (Gridnev et al. 2009). If the contribution of CMR-induced dielectric constant (ε) is large as compared to the stress-induced effect, the MC would be positive. On the other hand, MC would be negative for substantial contribution of stress-induced effect.

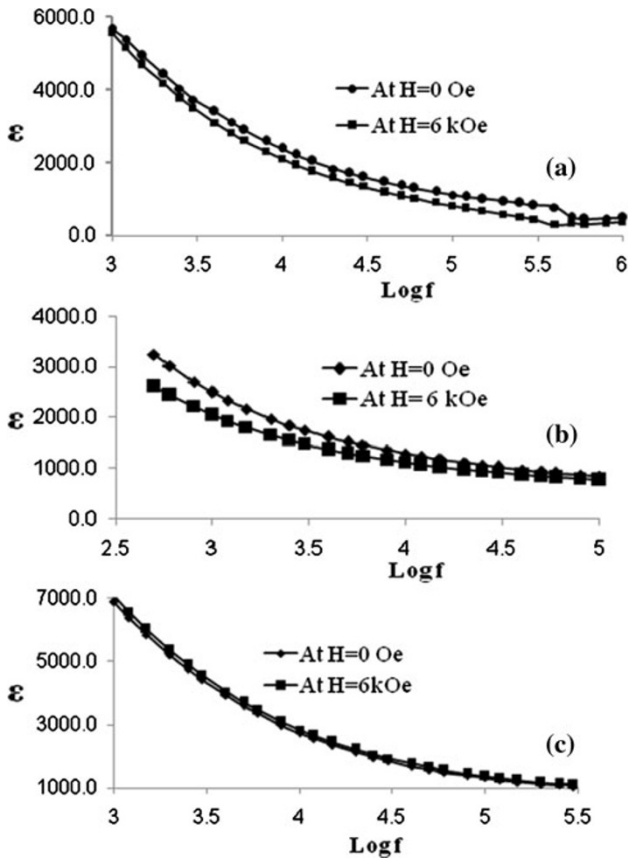

Fig. 3 **a** ε as a function of Log f for LBST0.20, $y = 0.2$ composite; **b** ε as a function of Log f for LBST0.25, $y = 0.1$ composite; and **c** ε as a function of Log f for LBST0.25, $y = 0.2$ composite

It is expected that the LSMO-BST forms 3–0 type connectivity between the LSMO and BST grains as the percentage of LSMO is <20 %. Therefore, the contribution of interfacial polarization would be large for $y = 0.2$ as compared to $y = 0.1$. Further, the contribution of piezoelectric effect will be significant for the LBST0.20 and LBST0.25 as compared to LBST0.30. These qualitative features are based on the basic theoretical model described by the Catalan for the CMR induced and Gridnev for stress-induced effect (Catalan 2006; Gridnev et al. 2009). Also, the observations on the parent BST system are taken into consideration to arrive at the qualitative logic mentioned above.

Figure 3c shows variation of ε as a function of log$F$ for LBST0.25 for $y = 0.2$ with and without applied magnetic field (H). It is observed that the ε shows a significant dispersion at low frequency and ε is almost constant for intermediate frequencies. Further, the ε passes through a broad maximum for F in the vicinity of 500 kHz. This frequency is expected to be EMR frequency because of the radial mode of oscillations of the pellet. As a confirmation of this prediction, variation of tanδ as a function of log$F$ is determined for all the LBST composites. Figure 4a, b shows the variation of tanδ versus log$F$ for LBST0.20 ($y = 0.2$) and LBST0.30 ($y = 0.1$), respectively. It is observed that the tanδ also becomes maximum at the EMR frequency of nearly 500 kHz. Further, as seen from Fig. 3a, c, the ε decreases with increase in H, while the ε for LBST0.25 and $y = 0.2$ increases with increase in H. This behavior is a typical feature of stress-induced change in ε as observed by Gridnev. Table 2 shows the variation of MC for LBST0.20, LBST0.25 and LBST0.30 for $y = 0.1$ and 0.2 at different frequencies. The magnitudes of MC are negative for LBST0.20 and LBST0.25 and $y = 0.1$, while magnitudes of MC are positive for LBST0.25 and LBST0.30 and $y = 0.2$. The positive MC is a typical feature of Catalan type contribution. It is observed that for $y = 0.1$, the stress-induced phenomenon plays its role, probably because of the lesser contribution of the LSMO phase. For $y = 0.2$, the LBST0.20 shows a negative and largest MC, while LBST0.25 and LBST0.30 show positive

MC. The positive MC would be significant for $y = 0.2$ and for the BST composition where piezo electric constant (d) becomes comparatively low. From Table 2, it is seen that positive magnitude of MC is also significant in the present case as the compositions of BST and LSMO possess T_c in the vicinity just above RT.

These features could be further understood by analysing the impedance spectra of the MD composites. Here Fig. 5a, b, respectively, shows the variation of Z'' as a function of Z' for LBST0.20, $y = 0.1$ and 0.2 both for with and without applied magnetic field (H). For $y = 0.2$, there exists a significant drop in the impedance curve (Kulkarni et al. 2009), while for $y = 0.1$ a significant contribution of interfacial polarization is seen in the impedance spectra. Here the drop center parameter A signifies the distribution in the RC time constant of the dielectric material and is defined through the relation $A = 2\theta/\pi$, where θ represents the drop center angle of the cole–cole plot (Choudhary and Thakur 2004). As the contribution of interfacial polarization is predominant at low frequencies, the impedance spectra are corrected for the presence of the interfacial polarization C_i for $y = 0.1$. The observed behavior could be understood in terms of a model as shown in Fig. 6. Here the parallel RC circuit represents the overall ε of the bulk, while the series capacitance C_i represents the contribution of interfacial polarization. It is also expected that for significant contribution of the piezo electric coupling, the bulk capacitance (C) will vary with applied (H), while for significant contribution of interfacial polarization, the drop center (A) or C_i would change with H. Table 3 shows the variation of C_i, R and C for LBST0.20, LBST0.25 and LBST0.30 and $y = 0.1$, 0.2, where R is the bulk resistance. The overall observations from the Table 3 are as below.

For $y = 0.1$, the drop center is nearly equal to zero, while for $y = 0.2$, drop center is significant. The C changes with H for LBST0.20, $y = 0.2$, where the contribution of the stress-induced change in polarization is predominant,

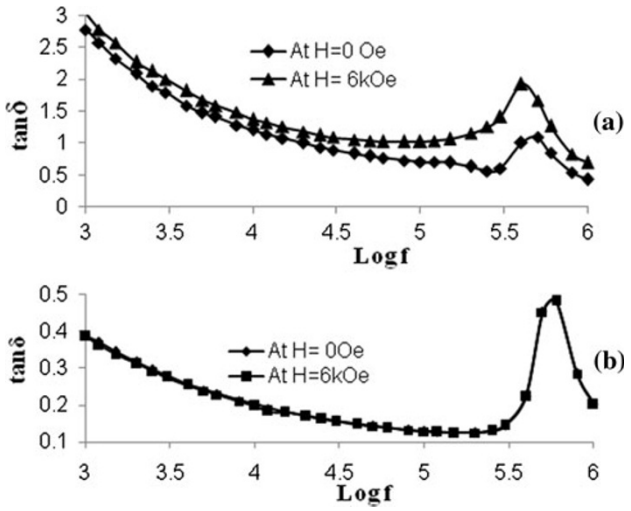

Fig. 4 **a** tanδ as a function of Log f for LBST0.20, $y = 0.2$ composite; **b** tanδ as a function of Log f for LBST0.30, $y = 0.1$ composite

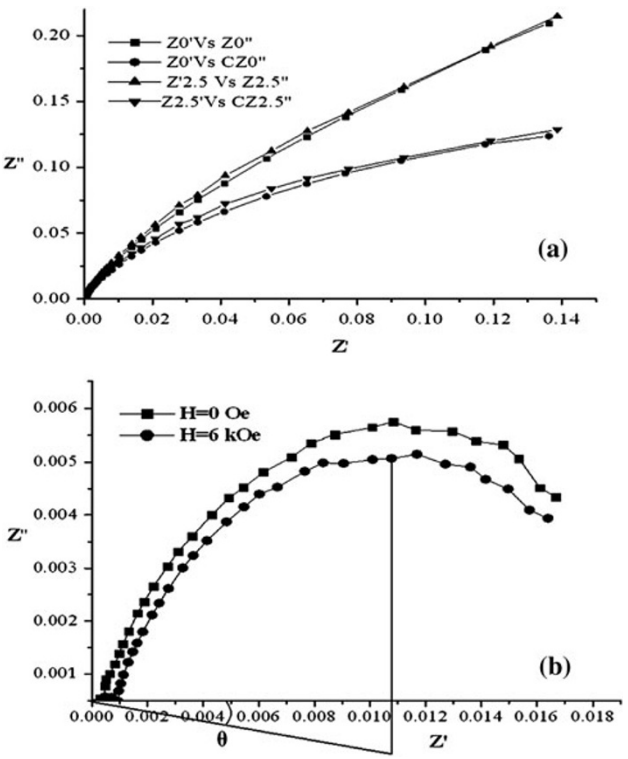

Fig. 5 **a** Variation of Z'' as a function of Z' for LBST0.20, $y = 0.1$; and **b** variation of Z'' as a function of Z' for LBST0.20, $y = 0.2$ composite

Table 2 Variation of magneto-capacitance (MC) for LBST0.20, LBST0.25 and LBST0.30, $y = 0.1$ and 0.2 composites

Frequency (F)	MC for LBST0.20		MC for LBST0.25		MC for LBST0.30	
	0.1 (%)	0.2 (%)	0.1 (%)	0.2 (%)	0.1 (%)	0.2 (%)
1 kHz	−2	−8.35	−17.66	+2.8	−0.82	+1.37
10 kHz	−2.36	−19.55	−13.41	+3.7	−0.66	+1.40
100 kHz	−2.12	−28.90	−7.84	+3.4	−0.78	+0.52
500 kHz	−1.57	−34.88	−2.91	+6.1	−0.1	+0.7
1 MHz	−1.56	−25.00	−7.49	+4.1	−0.52	+0.82

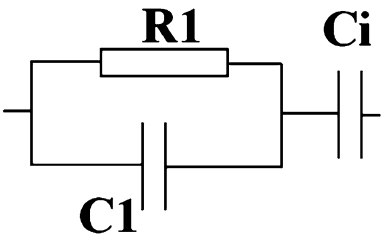

Fig. 6 Model circuit for BST-LSMO system

Table 3 Variation of interfacial capacitance, magnitudes of bulk resistance and bulk capacitance in model circuit for LBST0.20, LBST0.25 and LBST0.30 for y = 0.1 and 0.2 composites

Composites	y	H (kOe)	C_i (pf)	R (kΩ)	C (pf)
LBST0.20	0.1	0	3,698	272	1,169
		6	3,690	277	1,148
	0.2	0	–	33.3	9,563
		6	–	32.8	9,709
LBST0.25	0.1	0	9,838	162.4	1,161
		6	9,090	195.4	1,629
	0.2	0	–	27.8	11,450
		6	–	27.1	11,750
LBST0.30	0.1	0	1,260	448	710
		6	1,169	453	702
	0.2	0	14,540	494	644
		6	11,490	485	650

H applied dc magnetic field, C_i interfacial capacitance, R and C magnitudes of bulk resistance and bulk capacitance in model circuit for LBST0.20, LBST0.25 and LBST0.30 and $y = 0.1$, 0.2 composites

while the C_i changes significantly for LBST0.25 and LBST0.30 for $y = 0.2$, where the contribution of change in ε due to CMR-induced effect is significant. The parameters of LBST0.25 show the variation in the C_i as well as in C with H for both $y = 0.1$ and 0.2. These observations confirm the simultaneous presence of the Catalan type and Gridnev type contributions in the impedance spectra. Thus the observed impedance spectra and the associated model correctly explain the variation of MC for the LBST composites.

Conclusions

It is observed that the hydroxide co-precipitation route could be successfully used to form nanoparticles of both the BST and LSMO compositions. The initial particle size of the BST is observed to be in the range of 49–65 nm and for LSMO it is observed to be nearly 67 nm. It was observed that the BST compositions correctly reproduce the dielectric properties inconcurrence with the recently reported behavior (Ianculescu et al. 2008). The MD properties of these systems are observed to be interesting and the Catalan type contribution is observed significant for LBST0.25, where the BST0.25 possess a ferro to paraelectric transition just above RT. The observed magnitude of the MC is fairly large with a maximum value equal to −34 % for LBST0.20 and $y = 0.2$. The Gridnev type contribution is significant and large for LBST0.25, where BST0.25 has a ferro to paraelectric transition well above the RT and the material is strongly ferroelectric.

Acknowledgments The authors wish to thank Dr. V.R. Reddy, UGC-DAE-CSR Indore for his kind help during the course of this work. Also one of the authors MMS express their sincere thanks to University Grant Commission, New Delhi, India, for a Teacher Research Fellowship award under FIP, XIth Plan 2007-12.

References

Bidaut O, Goux P, Chikech MK, Belkaoumi M, Manglion M (1994) Space charge relaxation in perovskite. Phys Rev B 49:7868–7873

Catalan G (2006) Magnetodielectric effect without ferroelectric coupling. Phys Lett 88:102902

Chien A, Xu TX, Kim JH, Sachleben J, Speck JS, Lange FF (1999) Electrical characterization of $BaTiO_3$ heteroepitaxial thin films by hydrothermal synthesis. J Mater Res 14:3330

Choi SK, Kang BS, Cho YW, Vysochanskii YM (2004) Diffused dielectric anamoly in ferroelectric materials. J Electroceram 13:493–502

Choudhary RNP, Thakur Awalendra K (2004) Complex impedance analysis: a tool for ferroelectric materials. In: Proceeding of NSFD-XIII, pp 287–293

Fuck D, Dorman S (2006) Concentration phase diagram of $Ba_xSr_{1-x}TiO_3$ solid solutions. Phys Rev B 73:104116

Gridnev SA, Kalgin AV, Chernykh VA (2009) Magnetodielectric effect in two layer magnetoelectric PZT-MZF composite. Integra Ferroelectr 109:70–75

Haeni JH, Irvin P, Chang W, Ucker R et al (2004) Room temperature ferroelectricity in strained $SrTiO_3$. Nature 140:758–760

Ianculescu A, Berger D, Mitoşeriu L, Curecheriu LP, Drăgan N, Vasile E (2008) Properties of Ba_{1-x} Sr_x TiO_3 ceramics prepared by the modified-pechini method. Ferroelectrics 369(1):22–34

Jain M, Mujumdar SB, Katiyar RS, Bhalla AS (2003) Novel barium strotium titanate $Ba_{0.5}Sr_{0.5}TiO_3$/MgO thin films composites for tunable microwave devices. Mater Lett 57:4232–4236

Jigajeni SR, Kulkarni SV, Kolekar YD, Kulkarni SB, Joshi PB (2010) $Co_{0.7}Mg_{0.3}Fe_{2-x}Mn_xO_4$-$Sr_{0.5}Ba_{0.5}Nb_2O_6$ magnetoelectric composites. J Alloy Compd 492:402–405

Kim CH, Myung Y, Cho YJ, Kim HS, Park S-H et al (2008) Elecrtic structure of vertically allined Mn doped $CoFe_2O_4$ nano wires and their applications as humidity sensors and photo detectors. J Phys Chem C 113:7885

Kulkarni SV, Veer SS, Salunkhe DJ, Kulkarni SB, Joshi PB (2009) Dielectric behavior, complex impedance spectroscopy and

magnetoelectric effect in MCFO-BT composites. Mater Sci Res India 6(2):521–530

Lee SK, Park TJ, Choi GJ, Koo KK, Sang Woo Kim (2003) Effects of KOH/BaTi and Ba/Ti ratios on synthesis of $BaTiO_3$ powder by coprecipitation/hydrothermal reaction. Mater Chem Phys 82:742–749

McCormick MA, Roeder RK, Slamovich EB (2001) Processing effects on the composition and dielectric properties of hydrothermally derived $Ba_xSr_{1-x}TiO_3$thin films. J Mater Res 16(4): 1200–1209

Shui Z, Xianlin D, Genshui YC, Zhu J, Tang X (2011) Contribution of the magnetostriction and magnetoresistance to the room temperature magnetodielectric response in multiferroic composite thin films. Solid state commun 151:982–984

Tagantsev AK, Sherman VO, Astafiev KF, Venkatesh J, Setter N (2003) Materials for microwave tunable applications. J Electroceram 11:5–66

Tang Y-K, Sui Y, Xu D-P, Quin Z-N, Su W-H (2006) Study of magnetoresistance in nanostructured $La_{2/3}Sr_{1/3}MnO_3$ powder compacts. J Mag M Mater 299(2):260–264

Urushibara A, Moritomo Y, Arima T, Asamitsu A, Kido G, Tokura Y (1995) Insulator-metal transition and giant magnetoresistance in $La_{1-x}Sr_xMnO_3$. Phys Rev B 51:103–109

Veer SS, Salunkhe DJ, Kulkarni SV, Kulkarni SB, Joshi PB (2008) Effect of sintering aid on physical and magnetoelectric properties of $La_{0.70}sr_{0.30}MnO_3$–$BaTiO_3$ composites. Indian J Eng Mater Sci 15:121–125

Zimmerman F, Voiats M, Enesklou W, Ivezs-Tiffee E (2004) $Ba_{0.6}Sr_{0.4}TiO_3$ and $BaZr_{0.3}Ti_{0.7}O_3$ thick films as a tunable microwave dielectrics. J Euro Ceram Soci 24:1729–1733